Implementing Stretch Reflex in Musculoskeletal Robots Driven by Pneumatic Artificial Muscles Using Nonlinear Spring Model*

Mizuki Yoshida**, Wang Junqi**, Takumi Kawasetsu** and Koh Hosoda**

***Abstract*— This paper introduces a method to realize stretch reflexes in musculoskeletal robots without length sensors. The PAM was modeled as a nonlinear spring with a spring constant dependent on deformation and pressure. The dimension of the spring constant had physical bases in prior research, and its coefficients were derived from static tensile tests that measured force and length under a constant pressure. We applied the model to estimate the length of four PAMs with different materials and shapes, verifying the general applicability. When incorporated into an arm driven by antagonistic muscles, the model was proved effective in monitoring the velocity change of PAM length and triggering the stretch reflex, enhancing the robot's adaptability to disturbances. The reflex trajectory with a conventional sensor was well replicated with the model, offering a practical alternative to length sensors.**

I. INTRODUCTION

Soft robots are expected to be adaptive to the environment like living organisms [1]. They have already been developed to coexist with humans [2], and used to understand biological intelligence through a constructive methodology [3, 4]. As actuators in musculoskeletal robots, a pneumatic artificial muscle (PAM) is a popular solution [5]. PAMs have several advantages over conventional actuators such as a superior power-to-mass ratio [6], high compliance [7], and low cost and ease of production [8]. However, PAMs are nonlinear, which places heavy computational demands on a central control system. To overcome this hurdle, it is proposed to integrate reflex mechanisms found in living organisms into musculoskeletal robots [9]. Reflex mechanisms provide local control for swiftly responding to environmental changes without commands from the central control system, thereby reducing its computational load. One of the reflex mechanisms in the human body, a stretch reflex, detects the sudden change of muscle length [10] and protects the muscle from overstretching.

This paper presents a method to realize the stretch reflex in musculoskeletal robots without length sensors. A PAM was modeled as a nonlinear spring, and its length was estimated as the sum of natural length and deformation. The spring constant was defined as a function of pressure and deformation, with its dimension based on previous research and its coefficients determined experimentally. The general applicability of the model was validated through dynamic length estimation experiments across different materials and shapes of PAMs. The model was subsequently incorporated into the stretch reflex mechanism and required to maintain a robot arm in a fixed position while the falling mass generated an impact. The dynamic response of the reflex with the model was then compared to that with a conventional sensor.

The need for a sensorless approach stems from considerable challenges involved in directly measuring length of PAMs [11]. First, since a reflex action occurs instantaneously, it might lead to significant problems such as slackness in a wire encoder or interruption of the light beam from a laser sensor, which could prevent accurate measurement of the PAM's length. Second, because a length sensor needs to be posed at both PAM's ends, it could limit robot design. Third, sensor stiffness could impair the flexibility of the PAM. On the other hand, employing theoretical models of the PAM is equally challenging as these models often rely on nearly immeasurable parameters such as the total length of braided fibers or their braiding angle [12]. However, our approach overcomes this limitation by experimentally determining coefficients for each PAM and thus reflecting their characteristics. Applying our model not only offers broad applicability to PAMs of various materials and shapes, but also allows the sensors to gather at one end of a PAM, simplifying the robotic design.

II. MODEL FOR LENGTH ESTIMATION

Regarding a PAM as a spring [13], its length is expressed as the sum of natural length and deformation

$$l = l_n + d \tag{1}$$

where l is PAM length, l_n is natural length, defined as length with no external force at pressure p, and d is deformation from natural length, respectively.

Assuming that l_n is a linear function of p within a certain pressure range, it can be given as

$$l_n = mp + h \tag{2}$$

where m and h can be determined by static tensile tests.

Introducing the PAM's nonlinearity into the spring and assuming that the spring constant is the function of p and d, the force f is given by

$$f = (a_3 pd + a_2 p + a_1 d + a_0)d \tag{3}$$

The terms pd^2 and d^2 can be found in Chou et al.'s fundamental model [14], which capture the essential dynamic properties of the PAM. The term pd comes from Tondu et

*This work was supported by JSPS KAKENHI Grant Number JP23K18494

**Mizuki Yoshida, Wang Junqi, Takumi Kawasetsu and Koh Hosoda are with Department of Mechanical Engineering and Science, Graduate School of Engineering, Kyoto University, Kyoto, Japan
email: yoshida.mizuki.68s@st.kyoto-u.ac.jp, wang.junqi.77a@st.kyto-u.ac.jp, kawasetsu.takumi.2f@kyoto-u.ac.jp, hosoda.koh.7p@kyoto-u.ac.jp

al.'s model [15] to more accurately reflect differences in the shape of the PAM. The term d is added based on Ferraresi et al.'s model [16] to account for differences in material. The constants $a_0 \sim a_3$ in Eq. (3) are determined by the static tensile tests, and based on them, d can be calculated from the measured p and f by solving Eq. (3).

To examine the effect of the dimension and the number of parameters in the model equation, quadratic Eq.(4) and cubic Eq. (5) were also adapted, and the estimation errors were compared with those of the original model equation.

$$f = (b_5 p^2 + b_4 pd + b_3 d^2 + b_2 p + b_1 d + b_0)d \quad (4)$$

$$f = (c_4 p^3 + c_3 p^2 d + c_2 p d^2 + c_1 d^2 + c_0)d \quad (5)$$

III. EXPERIMENTAL METHOD

A. Parameter Identification

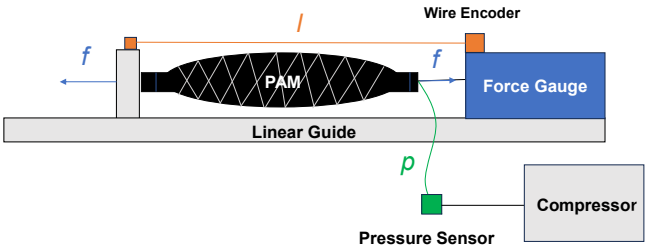

Fig. 1: Outline Diagram of Static Tensile Test

Fig. 1 is an outline diagram of the static tensile test to identify the parameters m, h, and a_i. Table I lists the shapes and materials of the four experimented PAMs (A,B,C,D). The experimental procedure was as follows. First, pressure p was adjusted to a constant level. Considering the strength of the materials, pressure of PAM-A, PAM-B, or PAM-C was adjusted to 0.4 MPa, 0.5 MPa, 0.6 MPa, 0.7MPa or 0.8 MPa, while pressure of PAM-D was 0.2 MPa, 0.3 MPa, 0.4 MPa, 0.5 MPa, or 0.6 MPa. Next, the PAM was gradually stretched from natural length l_n by 2.5 mm increments, and deformation d and force f were measured at each point. Each value was stabilized by waiting for at least 2 seconds after deformation. Once d reached its maximum value predetermined based on each PAM's strength, it was contracted to l_n by 2.5mm decrements, and d and f were measured again at each point. Finally, the parameters m, h, and a_i were calculated by the least squares method. The adapted pressure sensor was PSE540 (SMC Co.), the linear encoder was DS-025 (MUTOH INDUSTRIES Co. Ltd.), and the force gauge was FGP-5 (Nidec Co.).

TABLE I: Characteristics of Experimented PAMs

PAM	Length [mm]	Diameter [mm]	bladder Material
A	216	19.9	Rubber
B	211	13.4	Rubber
C	141	13.4	Rubber
D	212	19.0	Silicon
Agonist	180	16.0	Rubber
Antagonist	180	16.1	Rubber

B. Dynamic Length Estimation

We dynamically estimated length of the four PAMs to verify general applicability of the model. A jig holding the left end of a PAM in Fig. 1 was replaced with a pulley, and a proportional control valve was installed between the pressure sensor and a compressor. The experimental procedure was as follows. First, a weight of either 5 kg or 10 kg was connected to the PAM via the pulley to apply a constant force. Next, considering the strength of each PAM, the pressure p[MPa] was varied over time t[s] by the proportional control valve according to

$$p = 0.2 \sin\left(\frac{2\pi t}{5}\right) + 0.6 \quad (6)$$

for PAM-A, PAM-B, and PAM-C, and

$$p = 0.2 \sin\left(\frac{2\pi t}{5}\right) + 0.4 \quad (7)$$

for PAM-D. At each time, f, p, and the length l were measured. Finally, the errors were calculated between the measured and estimated length.

C. Reaching Task

We conducted reaching experiments to see errors when the model is actually incorporated into a robot arm. The system developed by Takahashi et al. [9] was adapted and positioned vertically. The system consisted of an arm with a pair of PAMs, an agonist muscle and an antagonist, and their shapes and materials are listed in Table I. The PAMs were connected to the arm with fishing line via shafts, and foil strain gauges (KFP-5-120-C1-65L1M2R, Kyowa Electronic Instrument Co. Ltd.) based on acrylic boards were attached to one end of each PAM.To validate the performance of the model in comparison with a conventional method, we wrapped the PAMs with conductive fiber sensors developed by Hitzmann et al. [17], which assesses the rate of change in length by detecting variations in resistance and thereby calculating the rate of change in diameter. The reaching movement was achieved by linearly increasing the pressure of the agonist muscle from 0.2 MPa to 0.6 MPa while simultaneously decreasing the pressure of the antagonist from 0.6 MPa to 0.2 MPa. During the reaching movement, the length of the PAM was measured with the linear encoder while it was estimated by the model and the fiber sensor, and the errors were calculated. The experiment time was 12 s, and the sampling frequency was set to 100 Hz.

During the experiment, the change in resistance of the strain gauges went to a quarter Wheatstone bridge circuit where three other resistors were $120 \pm 0.5\Omega$, and voltage signal from the circuit was converted to force according to Eq. (8). Eq. (8) assumes that voltage is a linear function of force because voltage of a Wheatstone bridge circuit is proportional to strain [18] and strain is proportional to force while material elastically deforms.

$$V = qf + V_{base} \quad (8)$$

V is the voltage signal from the strain gauge, q is the slope of voltage to force, and V_{base} is the voltage when no force is

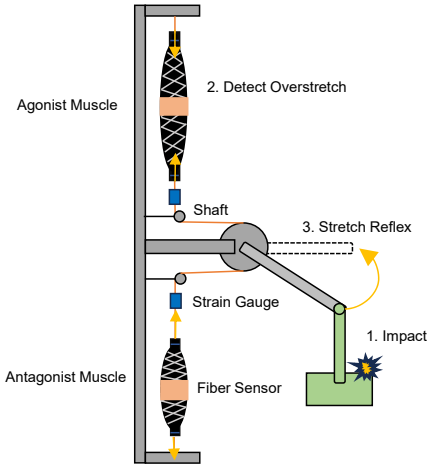

Fig. 2: Outline Diagram of Stretch Reflex Experiment

applied. The parameter q was obtained by measuring voltage and force while statically loading the strain gauge. Eq.(8) can be rewritten as

$$f = \frac{1}{q}\Delta V \tag{9}$$

where $\Delta V = V - V_{base}$. Substituting Eq. (9) into Eq. (3) gives

$$\Delta V = (a'_3 pd + a'_2 p + a'_1 d + a'_0)d \tag{10}$$

in which $a'_i = qa_i$, and the deformation d can be calculated by solving this equation.

D. Stretch Reflex

Fig. 2 is an outline diagram of the stretch reflex experiment. The arm was equipped with the basket and expected to keep it in a fixed position by maintaining the pressure of both PAMs at 0.4 MPa, and a 0.2 kg mass was dropped from a height of 14 cm to make an impact. During the experiment, velocities of the PAMs were calculated as

$$v_j = \frac{l_j - l_{j-1}}{dt} \tag{11}$$

where j is the sampling number, l_j is the estimated length, and dt is the sampling period. Since the system was set to 100 Hz, dt was 0.01 s. When the impact rapidly stretched the agonist PAM and its velocity exceeded a predetermined threshold, the stretch reflex was induced for 200 ms. The pressure command from the stretch reflex mechanism converged to the goal pressure from a top controller as follows

$$p_{ago} = p_{tp-ago} + \Delta p_{ago-exci} - \Delta p_{anta-inhi} \tag{12}$$

$$p_{anta} = p_{tp-anta} + \Delta p_{anta-exci} - \Delta p_{ago-inhi} \tag{13}$$

in which p_{tp} is the goal pressure from the top controller, Δp_{exci} is the excitatory pressure from the reflex mechanism, and Δp_{inhi} is the reciprocal inhibition pressure. Δp_{exci} and Δp_{inhi} were calculated by the following equation.

$$\Delta p_{exci} = \Delta p_{inhi} = kv \tag{14}$$

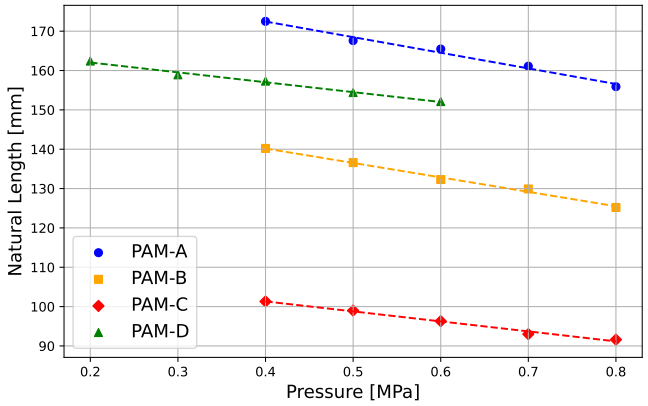

Fig. 3: Linearity of Natural Length to Pressure

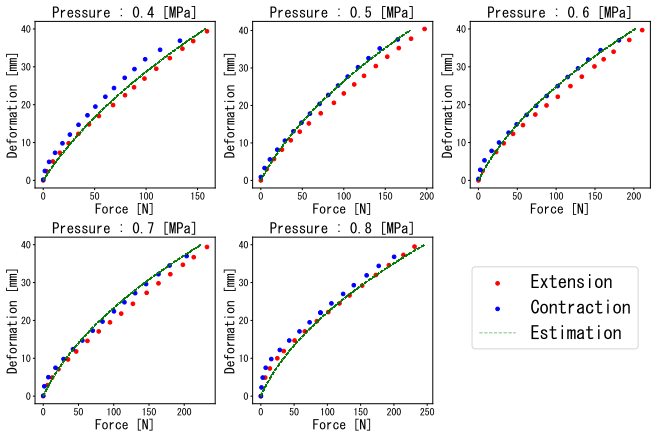

Fig. 4: Nonlinearity of Deformation under Different Pressure (PAM-B)

The velocity thresholds V_{thr} and the feedback gains k were predetermined experimentally as shown in Table II by assessing magnitude of impact from a falling mass. Takahashi et al. designed the reflex command Eq. (12) and Eq. (13) inspired by α motor neurons in human spinal cords [9]. The positioning tasks were conducted applying the stretch reflexes both with the model and the fiber sensor, and the reaction behaviors were compared.

TABLE II: Parameters for Stretch Reflex

PAM	V_{thr}[mm/s]	k[GPa · s]
Model	70	1/800
Fiber Sensor	25	1/300

IV. RESULT

A. Parameter Identification

Fig. 3 displays the relationship between pressure p and natural length l_n of the PAMs. As assumed, there is a tendency for l_n to decrease linearly with p within the tested pressure range. The dashed lines in Fig. 3 represent the fitted lines using the least squares method, as expressed by Eq. (2). Fig. 4 shows the result of the static tensile test for PAM-B. The red and blue points represent the measurements

during expansion and contraction respectively, and the green dashed lines represent the solutions d to Eq. (3), which is given by substituting the predetermined parameters a_i and the measured f and p. Generally, PAMs exhibit hysteresis caused by friction, so the data differ between expansion and contraction processes. Due to the space constraint, the result of the static tensile test is only presented for PAM-B, but similar results were obtained for the other PAMs.

B. Dynamic Length Estimation

Fig. 5 and Fig. 6 show the dynamic length estimation for PAM-B and PAM-D, respectively. With our model, with respect to the measurements by the linear encoder, the length estimation was achieved with maximum errors of 1.72 % for PAM-A, 1.19 % for PAM-B, 1.18 % for PAM-C, and 1.65 % for PAM-D respectively , and with root mean squared errors of 0.861 % for PAM-A, 0.653 % for PAM-B, 0.683 % for PAM-C, and 0.846 % for PAM-D respectively. When the model equation was switch to Eq. (4),the maximum errors were 1.12 % for PAM-A, 0.773 % for PAM-B, 1.01 % for PAM-C, and 0.755 % for PAM-D respectively, and root mean squared errors were 0.633 % for PAM-A, 0.353 % for PAM-B, 0.548 % for PAM-C, and 0.435 % for PAM-D respectively. When the model equation was switch to Eq. (5),the maximum errors were 1.22 % for PAM-A, 1.41 % for PAM-B, 0.951 % for PAM-C, and 1.99 % for PAM-D respectively, and root mean squared errors were 0.516 % for PAM-A, 0.484 % for PAM-B, 0.500 % for PAM-C, and 0.606 % for PAM-D respectively.

TABLE III: Error Percentages of Dynamic Length Estimation under Different Model Equations

PAM	A		B		C		D	
Model	Max Error	RMSE	Max Error	RMSE	Max Error	RMSE	Max Error	RMSE
Eq. (3)	1.72	0.861	1.19	0.653	1.18	0.683	1.65	0.846
Eq. (4)	1.12	0.633	0.773	0.353	1.01	0.548	0.755	0.435
Eq. (5)	1.22	0.516	1.41	0.484	0.951	0.500	1.99	0.606

C. Reaching Task

Table V shows the parameters for the length estimation of the agonist and antagonist muscles. The considerable difference in the voltage-force slope q between the two PAMs is attributable to the varying sensitivities of the handmade strain gauges.

Fig.7 displays the length estimation errors of the model and the fiber sensor in reaching task. Since the fiber sensor could only measure the rate of length change and not the absolute length, the estimation of absolute length by the fiber sensor was calibrated to the measurement of the linear encoder at the start of the reaching task. Therefore, it cannot be said that Fig.7 is exactly comparing the estimates from the model and the fiber sensor, but it serves as a reference for examining the accuracy of the model against the conventional sensor. The reaching task was performed five times for both the agonist and antagonist muscles. For the agonist muscle, with respect to the linear encoder measurement, the model showed a maximum error of 8.82 % with a root mean squared error of 5.24 %, while the fiber sensor showed a maximum error of 2.51 % with a root mean squared error of 0.888 %. For the antagonist muscle, the model showed a maximum error of 5.86 % with a root mean squared error of 5.02 %, while the fiber sensor showed a maximum error of 2.53 % with a root mean squared error of 1.78 %.

TABLE IV: Parameters for Length Estimation

PAM	m	h	a_3	a_2	a_1	a_0	q
Agonist	-60.1	170.1	-0.201	7.00	0.256	0.911	2.25×10^{-3}
Antagonist	-70.3	178.5	0.871	1.24	-0.129	22.4	4.33×10^{-3}

TABLE V: Error Percentages of Length Estimation in Reaching Task

PAM	Agonist		Antagonist	
Measurement	Max Error	RMSE	Max Error	RMSE
Model	8.82	5.24	5.86	5.02
Fiber Sensor	2.51	0.888	2.53	1.78

D. Stretch Reflex

Fig. 9 illustrates the dynamic behavior of the reflex with the model. The starting angle of the arm was -36 deg due to the basket's weight of 83.1 g. When the falling mass made an impact, the angle dropped dramatically, creating sudden soar in the voltage signal from the strain gauge and thus in estimated velocity. It went beyond the threshold and triggered the stretch reflex, leading to an increase in pressure in the agonist muscle and a decrease in the antagonist. The arm was then lifted back to the initial position, and after some oscillation, it settled down to a certain angle, holding the mass left in the basket.

Fig.8 displays the average and range of angles in 20 trials of the reflexes with the model and the fiber sensor. Since the thresholds and gains were determined experimentally, it is impossible to purely compare the behavior of the arm between the two reflexes, but it can be said that the reflex with the fiber sensor was well replicated with the model.

V. DISCUSSION

B. Dynamic Length Estimation

To improve the accuracy of length estimation, we expanded Eq. (3) by adding the terms p^2 and d^2 and increasing the parameters as follows

As a result, with respect to the measurements by the linear encoder, the dynamic length estimation was achieved with the maximum errors of 1.12 % for PAM-A, 0.773 % for PAM-B, 1.01 % for PAM-C, and 0.755 % for PAM-D respectively, and with root mean squared errors of 0.633 % for PAM-A, 0.353 % for PAM-B, 0.548 % for PAM-C, and 0.435 % for PAM-D respectively. The errors were reduced for all the PAMs as expected.

We also tried another approach by introducing a cubic polynomial model and increasing the parameters as follows

As predicted, the root mean squared errors decreased to 0.516 % for PAM-A, 0.484 % for PAM-B, 0.500 % for PAM-C, and 0.606 % for PAM-D respectively. However,

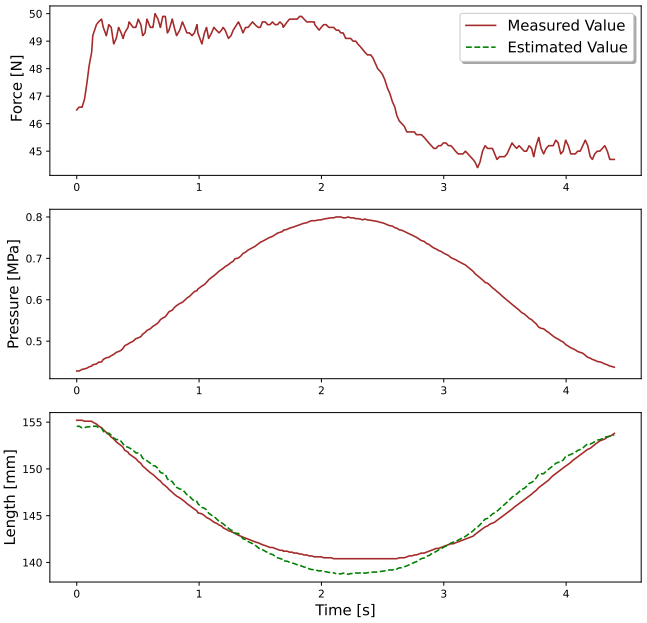

Fig. 5: Dynamic Length Estimation (PAM-B, Rubber)

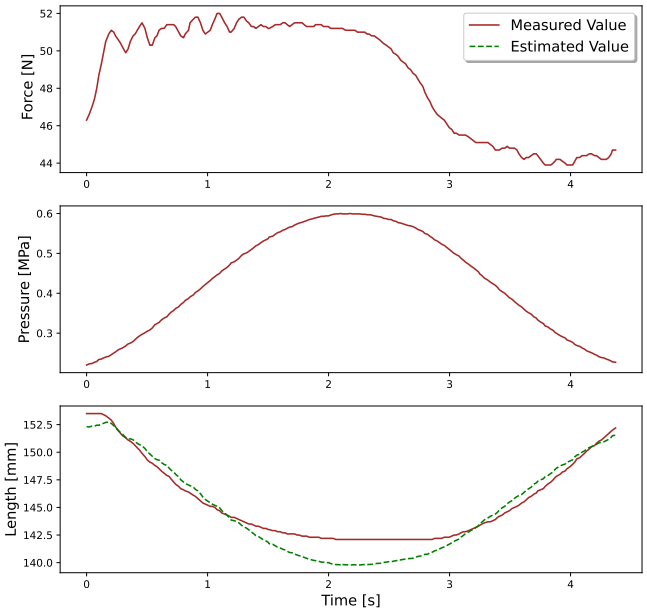

Fig. 6: Dynamic Length Estimation (PAM-D, Silicon)

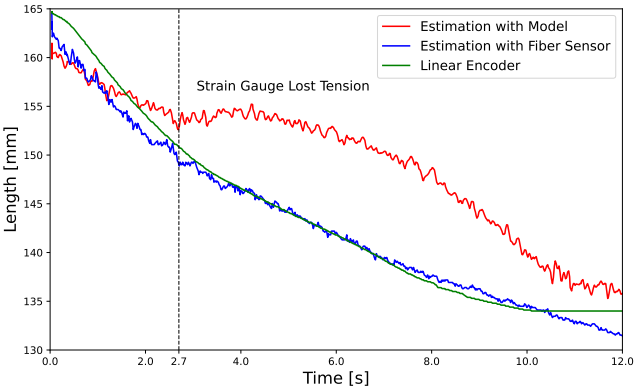

Fig. 7: Length Estimation Error in Reaching Task

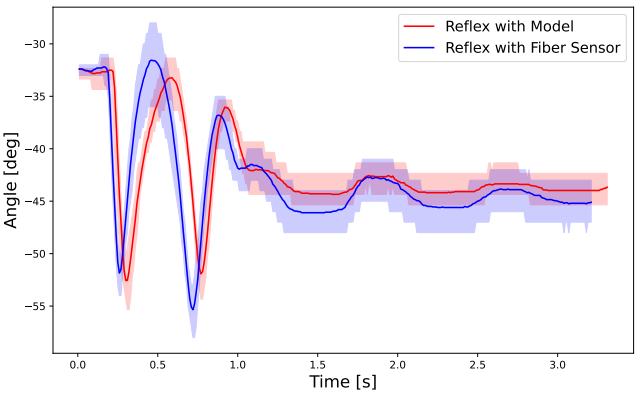

Fig. 8: Reflex Angle Similarity between Model and Fiber Sensor

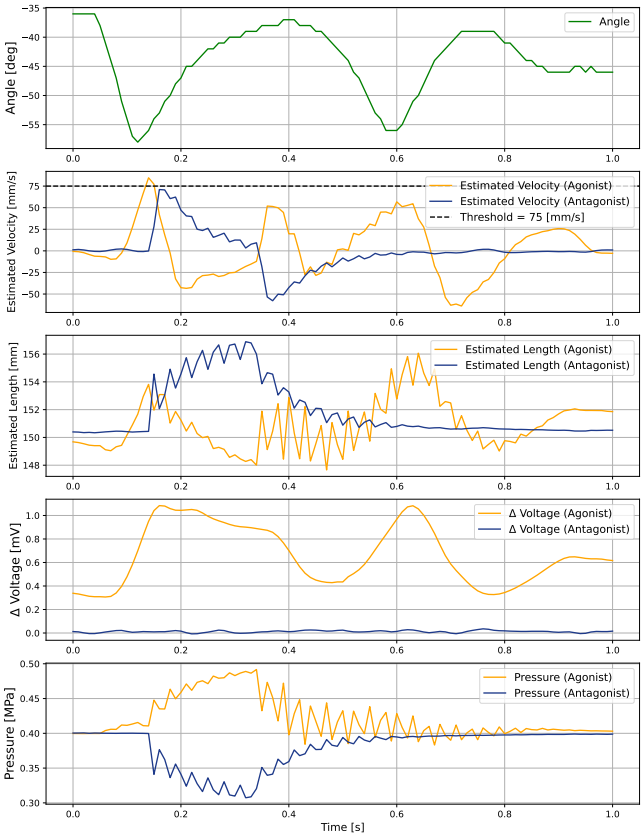

Fig. 9: Dynamic Behavior of Reflex with Model

even though the maximum errors decreased to 1.22 % for PAM-A and 0.951 % for PAM-C respectively, they actually increased to 1.41 % for PAM-B and 1.99 % for PAM-D respectively. This result suggests that, even if the coefficients

of the model equation are determined experimentally, the dimension must be carefully determined based on previous studies to accurately express intrinsic characteristics of the PAM. For example, the newly added term p^3 may have amplified the error of the pressure sensor. When applying the model to a reflex mechanism, it is also necessary to carefully consider the contribution of each term to the accuracy of the length estimation based on the reliability of the force and pressure sensors.

Wickramatunge et al. proposed separating the parameters a_i into contraction ones a_i^c and extension ones a_i^e to reflect the hysteresis of the PAM [13]. They also suggested using different parameters for low-pressure and high-pressure ranges to further improve the accuracy. However, our model did not adopt these suggestions and simplifies the length estimation method by using the same parameters across the entire pressure range, regardless of contraction or expansion. This is because our model is supposed to be adapted in a reflex mechanism. If the parameters have to be switched depending on the situation, it would be difficult for the reflex mechanism to respond quickly to disturbances. Musculoskeletal robots often carry microcomputers on their structures, so the employed length estimation method should be simple for efficient operation given the limited computational resources.

C. Reaching task

In the reaching task, the estimation errors with the model greatly increased compared to those in the dynamic length estimations in the previous section. This is because, as the PAM contracts, the fishing line loses contact with the shaft, resulting in slackness and failure to send voltage signals. As shown in Fig.7, the rate of change in length estimation with the model dropped around 2.7 second because the fishing line loses contact with the shaft and the deformation was estimated as zero from this point onward. In fact, for the agonist muscle, after the fishing line slackened, the maximum error grew significantly to 8.82 $\%$ with the root mean squared error of 5.94 $\%$, whereas before slacking, the errors were smaller with the maximum error of 2.99 $\%$, and the root mean squared error of 1.71 $\%$. Compared to the fiber sensor, the errors were still large even before slacking. One possible cause lies in the process of converting voltage to force. The voltage values fluctuated significantly due to slight positional shifts of the fishing line, and the error in the slope of voltage to force q might have been amplified during the estimation procedure.

The looseness of the strain gauge poses a disadvantage when it comes to continuously tracking length of the PAM, but it contributes to creating biomimetic behavior. In the human body, a muscle spindle is aligned parallel to a muscle and monitors change in its length, but when the muscle contracts, the muscle spindle becomes unloaded, leading to the cessation of neural discharging activity [19]. One of the ultimate goals of our research is to propose a possible operating principle of the reflex mechanism in the human body by mimicking it in a musculoskeletal robot. Our length estimation method is designed in pursuit of this purpose, hence it is desirable to develop a local control system that responds only when the muscle is suddenly stretched just as the human neural system does. In this sense, the errors during muscle contraction are not a primary concern.

D. Stretch Reflex

In the reflex experiment, since the fiber sensor directly measure diameter change of the PAM, it could accurately track length change and capture the impact as a spike in velocity. With our model, however, the fluctuations in the pressure sensor and the strain gauge were transmitted to the estimated length and thus the velocity was often overestimated, making it difficult to separate the impact clearly in the velocity field. This made it difficult to set the threshold and the feedback gain, thereby increasing the possibility of mistriggering the reflex or making the reflex to continue triggering itself. This issue might be mitigated by applying a low-pass filter to the estimated velocity.

In addition to the Ia reflex pathway that detects overstretch of a muscle with a muscle spindle, the human muscle has the Ib reflex pathway which perceives excessive tension with a Golgi tendon organ. Therefore, pressure sensors, tension sensors and length sensors are required to realize the coexistence of the two pathways in a musculoskeletal robot driven by PAMs. The advantage of our approach is that the length sensors can be removed by allocating its function to the pressure and tension sensors.

REFERENCES

[1] D. Rus and M. T. Tolley, "Design, Fabrication and Control of Soft Robots", *Nature*, vol. 521, pp. 467–475, 2015.

[2] H. Sato, K. Uchiyama, Y. Mano, F. Ito, S. Kurumaya, M. Okui, Y. Yamada, and T. Nakamura, "Development of a Compact Pneumatic Valve Using Rotational Motion for a Pneumatically Driven Mobile Robot With Periodic Motion in a Pipe", *IEEE Access*, vol. 9, pp. 165271–165285, 2021.

[3] K. Hosoda, S. Sekimoto, Y. Nishigori, S. Takamuku, and S. Ikemoto, "Anthropomorphic Muscular–Skeletal Robotic Upper Limb for Understanding Embodied Intelligence", *Advanced Robotics*, vol. 26, no. 7, pp. 729–744, 2012.

[4] A. D. Marchese, C. D. Onal, and D. Rus, "Autonomous Soft Robotic Fish Capable of Escape Maneuvers Using Fluidic Elastomer Actuators", *Soft Robotics*, vol. 1, no. 1, pp. 75–87, 2014.

[5] S. M. Mirvakili and I. W. Hunter, "Artificial Muscles: Mechanisms, Applications, and Challenges", *Advanced Materials*, vol. 30, no. 6, 2018.

[6] D. B. Reynolds, D. W. Repperger, C. A. Phillips, and G. Bandry, "Modeling the Dynamic Characteristics of Pneumatic Muscle", *Annals of Biomedical Engineering*, vol. 31, no. 3, pp. 310–317, 2003.

[7] C.-P. Chou and B. Hannaford, "Static and Dynamic Characteristics of McKibben Pneumatic Artificial Muscles",*Proceedings of the 1994 IEEE International Conference on Robotics and Automation*, pp. 281–286, IEEE Comput. Soc. Press, 1994.

[8] K. P. Ashwin and A. Ghosal, "A Survey on Static Modeling of Miniaturized Pneumatic Artificial Muscles With New Model and Experimental Results", *Applied Mechanics Reviews*, vol. 70, no. 4, 2018.

[9] R. Takahashi, Y. Wang, J. Wang, Y. Jiang, and K. Hosoda, "Implementation of Basic Reflex Functions on Musculoskeletal Robots Driven by Pneumatic Artificial Muscles",*IEEE Robotics and Automation Letters*, vol. 8, no. 4, pp. 1920–1926, 2023.

[10] E. R. Kandel, J. H. Schwartz, T. M. Jessell, S. Siegelbaum, A. J. Hudspeth, S. Mack et al., "Principles of Neural Science", McGraw-Hill, vol. 4, 2000.

[11] R. Sakurai, M. Nishida, H. Sakurai, Y. Wakao, N. Akashi, Y. Kuniyoshi, Y. Minami, and K. Nakajima, "Emulating a Sensor Using Soft Material Dynamics: A Reservoir Computing Approach to Pneumatic Artificial Muscle", *2020 3rd IEEE International Conference on Soft Robotics (RoboSoft)*, pp. 710–717, 2020.

[12] T. Nozaki and T. Noritsugu, "Motion Analysis of McKibben Type Pneumatic Rubber Artificial Muscle with Finite Element Method", *International Journal of Automation Technology*, vol. 8, pp. 147–158, 2014.

[13] K. C. Wickramatunge and T. Leephakpreeda, "Empirical Modeling of Dynamic Behaviors of Pneumatic Artificial Muscle Actuators", *ISA Transactions*, vol. 52, no. 6, pp. 825–834, 2013.

[14] C.-P. Chou and B. Hannaford, "Measurement and Modeling of McKibben Pneumatic Artificial Muscles", *IEEE Transactions on Robotics and Automation*, vol. 12, no. 1, pp. 90–102, 1996.

[15] B. Tondu and P. Lopez, "Modeling and Control of McKibben Artificial Muscle Robot Actuators", *IEEE Control Systems*, vol. 20, no. 2, pp. 15–38, 2000.

[16] W. F. Carlo Ferraresi and A. Manuello, "Flexible Pneumatic Actuators: A Comparison between The McKibben and the Straight Fibres Muscles", *Journal of Robotics and Mechatronics*, vol. 13, no. 1, pp. 56–63, 2001.

[17] A. Hitzmann, Y. Wang, T. Kessler, and K. Hosoda, "Using conductive fabrics as inflation sensors for pneumatic artificial muscles", *Advanced Robotics*, pp. 1–17, 2021.

[18] K. Hoffmann, "Applying the Wheatstone Bridge Circuit," HMB Germany, 1974.

[19] C. C. Hunt and S. W. Kuffler, "Stretch Receptor Discharges during Muscle Contraction," *The Journal of Physiology*, vol. 113, no. 2-3, pp. 298–315, 1951.